Vibratory response of planetary gear sets housing by a spectral iterative approach – Modulation effects induced by carrier rotation

Jessica Neufond [1], **Joël Perret-Liaudet** [2], **Emmanuel Rigaud** [2], **Pascal Bouvet** [1]

[1] Vibratec SA, 69130, Ecully, France, jessica.neufond@vibratec.fr
[2] Laboratoire de Tribologie et Dynamique des Systèmes (LTDS), UMR CNRS 5513, Ecole Centrale de Lyon, Université de Lyon, 36 Avenue Guy de Collongue, F69134 ECULLY cedex, France

Abstract

The main source of excitation at the origin of the vibratory response of gear system is generated by the meshing process, leading to the variation of the mesh stiffness and deviation between the ideal input/output transmission law and the real one. In planetary gear, these phenomena are amplified due to the presence of multiple meshes. Moreover, in operating, the varying relative position between the planets gears and the ring gear is at the origin of a modulation in the temporal response measured on a fixed point on the ring gear housing. The aim of this work is to present a novel method to investigate the dynamic behaviour of a planetary gear set. This method is a complete procedure for a planetary gear system whining noise computation induced by the multi-mesh excitations. This procedure is divided in three main steps. First, the parametrical internal excitations are simultaneously characterized by considering all contacts at the multiple gear meshings. Secondly, the coupled equations of motion are projected onto the modal basis and the stationary dynamic response is computed using an iterative spectral method. Finally, the modulated response of the planetary gear housing (ring gear) is evaluated. Numerical results are discussed and compared with experimental observations.

1 Introduction

Over the wide range of geared systems, the planetary gear sets are distinguished by their capacity to provide high gear ratio in a compact package. Indeed, a single stage planetary gear is composed of a central gear, called the sun, which meshes with N gears called planets, which mesh with a peripheral gear (with internal teeth) called the ring gear, while a carrier drives the axis of the planets. Thus, the sun, the ring gear and the carrier are three coaxial solids. Planetary gear sets are used for example in automatic gearboxes, transmissions for hybrid vehicles, energy production systems such as wind turbines, home automation applications such as shutters or blinds. However, contrary to cylindrical gears with fixed and parallel axes, whining noise prediction and control remains a difficult problem because of the coupling between the multiple gear meshes and the mobility of the planets axes.

It is well know that the gear whining noise is generated by the mesh process [1]. The problem posed is multi-scale in nature. Indeed, the overall dynamic and vibroacoustic behaviour of geared systems (on the scale of a meter) depends on the local micro-geometry of the teeth (on the scale of a micron), associated with the transmission error. Moreover, the problem is parametric in nature, due to the periodic fluctuation of the mesh stiffness, and non-linear, due to the presence of functional clearance and close contacts between teeth and bearings. These parametric internal excitations generate dynamic mesh forces which are transmitted to the housing through wheel bodies, shafts and bearings. In the end, the radiated noise is directly related tot he vibratory state [2, 3, 4].
In the case of planetary gear sets, housing vibratory state prediction is challenging. In many applications, the carrier rotation modulates the housing vibration response at its rotational frequency [5, 6], as a consequence of the successive passage of the planets. The iterative spectral method allows the solving of linear parametric equations of motion, in the carrier reference frame, in the spectral domain, with short computational time [7, 8]. The dynamic response at meshes is hence fully characterized and the short computational time allows parametric investigation. However, the computation of the dynamic response of any point on the ring gear requires an additional step. Even if many works deal with ring gear modulated dynamic response [9] [10], further work is required to include modal behaviour contribution of the ring gear. Indeed, these existing methods propose a simplified formulation based on the use of Hanning window functions to simulate the growth/decay of the vibratory amplitude as one planet

approaches or moves away from the measured point. Though these approach give good correlation with experiments at low frequencies, the coincidence between mesh frequencies and housing modes at higher frequencies is less discussed. Thus, a novel approach is proposed by taking into account the modulation effects induced by the relative rotation between the observation point (fixed point located on the ring gear) and the meshes (attached to the carrier reference frame). Numerical results are analysed and compared with experimental data.

Figure 1: Example of modulated housing vibratory response of a planetary gear with three planets, computed using Hanning and Heaviside functions [9]

2 Numerical model

This paper proposes a novel approach to predict the vibroacoustic behaviour of planetary gear sets, from evaluation to the internal parametric excitations and their coupling to the housing vibratory state. The focus is set on how to calculate the modulation effects due to the relative motion between the axis of the planets and the ring gear, using a finite element approach and a spectral iterative method. This procedure can be divided into three main steps. First, static transmission error and mesh stiffness fluctuation at each meshes are computing through the solving of contact equations. Next, the computation of the dynamic response of the drive train is performed through an iterative spectral method. Finally, the dynamic response of the housing is computing through the relative rotation between the observation point (fixed point located on the housing) and the meshes (attached to the carrier rotating reference frame).

2.1 Static transmission error and mesh stiffnesses fluctuation

Assuming infinitely rigid and geometrically perfect gears, their circular involute profile offers a constant instantaneous transmission ratio. However, these undeformable and geometrical assumptions are never met. Geometrical errors or tooth corrections as well as deformation under torque, induce a fluctuation of the instantaneous reduction ratio around its theoretical value. This fluctuation results in the so-called static transmission error (STE). It is defined as the deviation between the actual position of the output shaft and its theoretical position [1, 2]. The calculation of the STE is well mastered. It is based on the resolution of the equations describing the static contact between the gear teeth (see for example Tavakoli et al. [11] and Rigaud et al. ([12]). For each position θ of the driving gear, the contact between the teeth are established based on a kinematic analysis which assumes a geometrically perfect and infinitely rigid mechanism, leading to the theoretical contact line on the tooth surfaces. The resolution of the contact equations leads to the evaluation of STE $\delta(\theta)$ and load distribution $\mathbf{P}$ along the contact line.

In the case of planetary gears, equations of contact are solved taking account of all the meshes simultaneously [13]. First, a planet gear is defined as reference. Contact points for the other gears are deduced for each successive angular position of the reference gear, by taking into account planets mesh phasing condition [14], which depends on the number of planets and the number of tooth of the sun gear.

With knowledge of contacts lines location between the sun and the planets, the contacts lines between ring and planets occur is deduced from geometrical construction. For each angular position θ of the driving wheel, a kinematic analysis allows the resolution of contact equations of each meshes $j = 1 : 2N$:

$$\begin{cases} \mathbf{H_j P_j} = \delta_j(\theta)\mathbf{1} - e_j \\ \mathbf{P_j} = F_j \end{cases} \tag{1}$$

At each contact, the constraints are:

$$\begin{cases} -\mathbf{H_j P_j} + \delta_j(\theta)\mathbf{1} \leq e_j \\ \mathbf{P_j} \geq F_j \end{cases} \tag{2}$$

With $\mathbf{H_j}$ the compliance matrix of contact j, $\mathbf{P_j}$ the vector of the load distribution on the contact line j. δ_j is the STE at mesh j, which correspond to a linear displacement of the gear related to the pinion along the line of action. $\mathbf{e_j}$ is the vector of the initial gaps between the contact surfaces determined from tooth modifications and manufacturing errors, F_j is the static load oriented along the line of action, induced by the input torque, and $\mathbf{1}$ is a unitary vector used for dimensional consideration.

In the case of a planetary gear train with N planets, the contact equations are solved by taking into account the $2N$ meshes simultaneously. For each planets, the overall STE Δ is introduced from the sum of the local sun-planet δ_n and planet-ring gear $\delta_{n'}$ STE:

$$\Delta = \delta_n + \delta_{n'} \tag{3}$$

Unlike cylindrical gears with fixed axes for which the static force transmitted by the teeth is an initial input data of the problem, the distribution of the driving torque between the teeth of the planetary gear sets (and thus of the force transmitted by each gear) is an unknown of the problem. This distribution depends on the flexibility of the elements in contact, on the initial distances between the teeth induced by the microgeometrical gaps, and on the phase conditions between the gears: in out of phase systems, the contact can be established between two pairs of teeth for a gear (sun-planet or planet-ring), whereas it is established between a single pair of teeth for another gear of the same nature. Thus, complementary constraint are added, acting that the total force is transmitted by the sun to the three planets and from the three planets to the ring, and all the force received by a planet from the sun are transmitted to the ring, so:

$$F_T = \sum_{n=1}^{N} F_n = \sum_{n'=N+1}^{2N} F'_n, \qquad F_n = F'_n \tag{4}$$

Furthermore, the instantaneous local mesh stiffness is defined from the derivative of the force transmitted by the mesh, in relation to the static transmission error, for each angular position θ_s of the driving gear and for each meshes:

$$k_j(\theta_s) = \frac{\partial F_j}{\partial \delta_j}(\theta_s) \tag{5}$$

2.2 Dynamic response of the kinematic chain by a spectral iterative method

The numerical procedure proposed in this paper is based on several main assumptions. The ring gear is assumed to be axisymmetric. Thus, the modal basis is independent of the angular position of the planets. As a result, one modal basis is enough for solving equations at each angular position. Futhermore, the equations of motion are first solved in a reference frame associated with the carrier, which is equivalent to considering that the ring gear is moving in this reference frame. In practice, the modal basis is computed, considering the carrier fixed. Indeed, the maximum relative speed of the ring gear to the carrier is about 12 m/s. This represents about 0.2% of the pressure wave propagation speed of 5200 rpm. Except for very high speed applications, gyroscopic and centrifugal effects can be neglected. This assumption is verified by the complex modal basis calculation (see equations detailed Cooley and Parker [15]), here performed for a carrier rotational [0-120] rad/s speed range. The results obtained show a negligible impact of gyroscopic effects. Less than 1% difference in eigenfrequencies is observed. Mode shapes are almost identical.

The dynamic model chosen is based on a finite element discretisation of the transmission. The dynamic response of the kinematic chain (i.e. dynamic transmission errors and teeth dynamic loads) can directly be computed in the carrier reference frame. Thus, the equations of motion are expressed from the linearised gear force:

$$\mathbf{M}_{EF}\ddot{x} + \mathbf{C}_{EF}\dot{x} + \mathbf{K}_{EF}x + \sum_{j=1}^{2N} k_j(t)\mathbf{R}_j\mathbf{R}_j^T x = \sum_{j=1}^{2N} k_j(t)\mathbf{R}_j\mathbf{R}_j^T x_s(t) \tag{6}$$

With $\mathbf{M}_{EF}$ and $\mathbf{K}_{EF}$ respectively the mass and stiffness matrix from the finite element model and $\mathbf{C}$ the damping matrix taken into account a posteriori with the modal decoupling hypothesis, through an equivalent viscous damping coefficient for each mode. The elastic coupling between gears is introduced via the periodic mesh stiffnesses $k_j(t)$, which results from the limited development of the first-order of tooth dynamic load. This coupling, which acts along the lines of action, involves vectors of geometrical structure $\mathbf{R}_j$. The vector x_s corresponds to the static response generated by the driving and brake torque, assumed constant. $\mathbf{R}_j^T x$ is the dynamic transmission error and $\mathbf{R}_j^T x_s$ the static transmission error.

The finite element model of the planetary gear is presented in Figure 2. The housing (with ring gear directly manufactured on), gears, input and output shafts and the carrier are modelled using 3D elements. The bearings are modelled using axial and radial spring elements. Inertia are used to model the presence of a motor and a break. These boundary inertia are connected to the input and output shafts with torsional stiffnesses, modelling the flexible couplings on test bench. Mesh stiffnesses mean values are included in the finite elements model for elastic coupling of the gears.

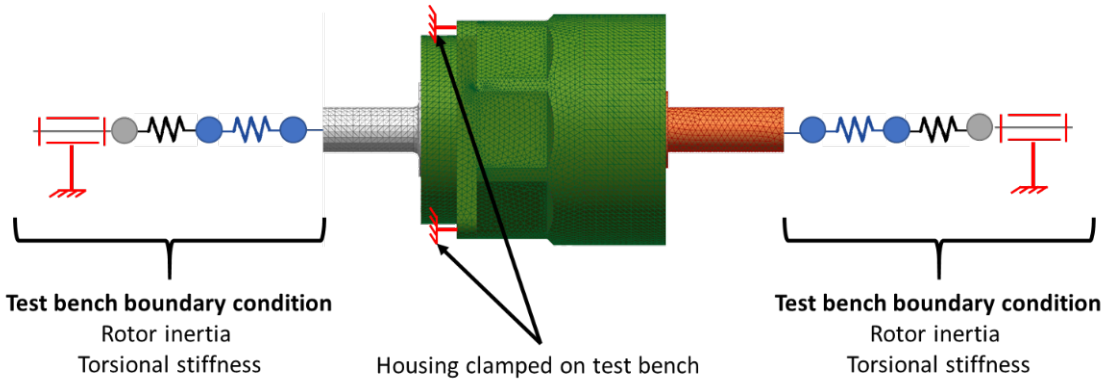

Figure 2: Finite elements model of the planetary gear

Time discretization methods lead to prohibitive calculation times. Low frequencies require long time period. High frequencies require fine time sampling. Hence, parametric equations of motions are solved using the spectral iterative method. The method is described in details in [7].It is based on the direct computation of the solutions in the spectral domain [7]. To this end, the matrix equation **??** is rewritten in the mean modal basis with $\mathbf{B}$, deduced from the eigenvalues problem $(\mathbf{K}_{EF} + \sum_{j=1}^{2N} k_j(t)\mathbf{R}_j\mathbf{R}_j^T) - \omega^2\mathbf{M}_{EF}$. By introducing the vector of modal coordinates $\mathbf{z}$ such as $\mathbf{x} = \mathbf{B}\,\mathbf{z}$, and thanks to the orthogonality property of the eigenmodes, equations in the modal basis can be written under the following index form:

$$\ddot{z}_k + 2\zeta_k\omega_k\dot{z}_k + \omega_k^2 z_k + \sum_{j=1}^{2N} g_j(t) r_{jk} \sum_{l=1}^{L} r_{jl} z_l = \sum_{j=1}^{2N} k_j(t) r_{jk} \delta_j^{(s)}(t) \tag{7}$$

In this equation, ζ_k is the equivalent viscous damping ratio of mode k, the term $r_{jk} = \mathbf{V}_k^T\mathbf{R}_j$ is the projected geometric structure vector in the modal basis and ωk is the k^{th} eigenvalues of the system. One should note that equations 7 remains coupled.

The first step of the iterative spectral method is based on solving the coupled equations of motion 7 in the spectral domain, retaining only the stationary part of the forced response of the system. Indeed, the parametric instabilities are characterised by an exponentially increasing free response. It is assumed that the viscous damping is sufficient to lie outside these regions of parametric instabilities and that it leads to an exponentially decreasing free response (asymptotic stability). Thus one can write:

$$Z_k(\omega) + H_k(\omega) \sum_{j=1}^{2N} G_j(\omega) r_{jk} \otimes \sum_{l=1}^{L} r_{jl} Z_l(\omega) = H_k(\omega) \sum_{j=1}^{2N} K_j(\omega) \otimes r_{jk} E_j^{(s)}(\omega) \tag{8}$$

where $Z_k(\omega)$, $G_j(\omega)$, $K_j(\omega)$ et $E_j^{(s)}(\omega)$ are respectively the Fourier transform of $z_k(t)$, $g_j(t)$, $k_j(t)$ et $\delta_j^{(s)}(t)$. The operator $\otimes$ represents the convolution product and $H_k(\omega)$ represents the complex frequency response function of the k mode, i.e.:

$$H_k(\omega) = \frac{1}{(\omega_k^2 - \omega^2 + 2i\zeta_k\omega_k\omega)} \tag{9}$$

After several judicious transformations, the iterative process can be written as follows:

$$E_i^{n+1}(\omega) = S_i(\omega) - \sum_{j=1}^{2N} T_{ij}(\omega) \cdot \left[G_j \otimes E_j^n \right](\omega) \tag{10}$$

with:

$$E_i^{(1)}(\omega) = S_i(\omega) \tag{11}$$

The stopping criterion is based on the relative difference between two iterations which is compared to a very small real ϵ, i.e. $\epsilon = 10^{-6}$:

$$\frac{||E_i^{n+1}(\omega) - E_i^n(\omega)||}{||E_i^{n+1}(\omega)||} < \epsilon \tag{12}$$

With the spectral iterative method, large systems of periodic differential equations can be solved, with minimal calculation times. Previous studies have demonstrated the validity of this method for multi-meshings systems [4], like planetary gear sets [16, 8].

2.3 Vibroacoustic response of the planetary gear housing

The dynamic response computation with the spectral iterative method allows to describe the vibratory state of any point of the finite element model. Even if this approach allows to directly compute the planetary gear chain dynamic response, one more step is needed to compute the response of any point on the ring gear. The carrier rotation modulates this response, as well as its rotational frequency [9]. The modulation is considered at posteriori, by taking into account the effect induced by the relative rotation between the observation point (fixed point located on the ring gear) and the meshes (attached to the carrier reference frame, as schematized in Figure 3.

The radial dynamic response of the cylindrical ring gear node n is noted $\tilde{u}_n(R, \psi_n, z, t)$, with R the external radius of the ring gear, z its axial position and t the time. The angular position of the observation point is noted ψ_n and in the carrier reference frame $(\overrightarrow{X}_c, \overrightarrow{Y}_c, \overrightarrow{Z}_c)$ and φ_n in the housing frame $(\overrightarrow{X}_r, \overrightarrow{Y}_r, \overrightarrow{Z}_r)$. The dynamic responses are computed by considering the system under load, without any relative movement between the ring gear and the carrier. In practice, the dynamic response $u_n(r, \varphi_n, z, t)$ of a fixed point on the ring gear (in relative motion to the carrier) is measured.

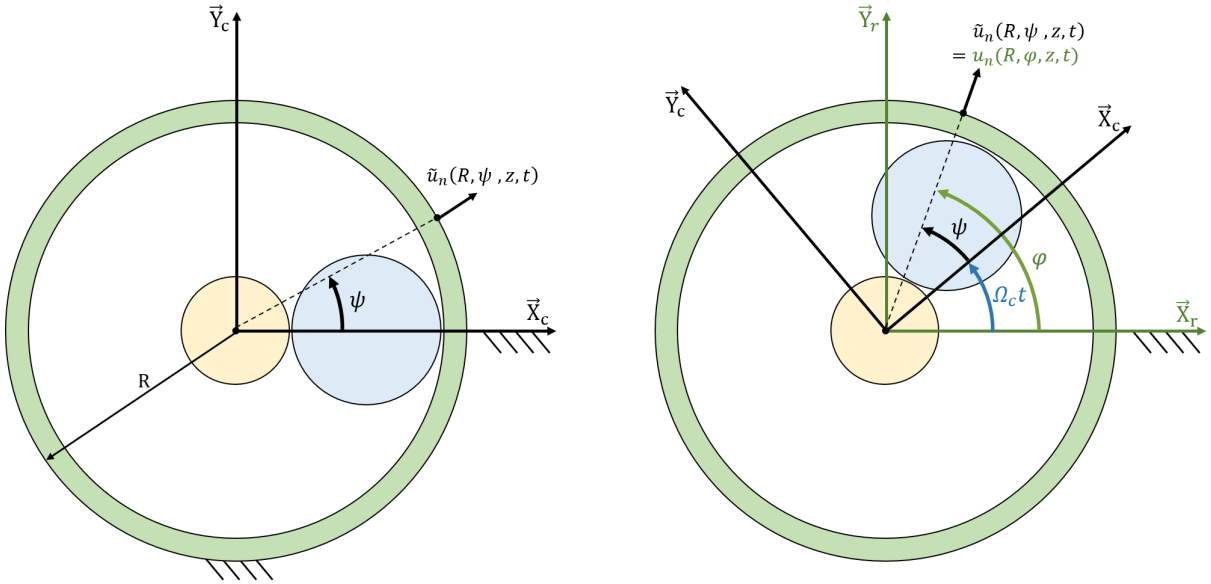

Figure 3: Model for the calculation of the dynamic response of a housing point

By properly choosing the initial position of the carrier at $t = 0$, one can write:

$$u_n(R,\varphi,z,t) = \tilde{u}_n(R,\psi,z,t) = \tilde{u}_n(R,\varphi_n - \Omega_c t,z,t) \tag{13}$$

Therefore, a point $B(R,\varphi_B,z_B)$ on the ring gear has a dynamic response out of phase from point $A(R,\varphi_A < \varphi_B, z_A = z_B)$ with a delay of:

$$t_B - t_A = -\frac{\varphi_B - \varphi_A}{\Omega_c} \tag{14}$$

With Ω_c the carrier angular rotational speed. Based on this description, we proposed to access the dynamic response $u_n(R,\varphi_n,z,t)$, a linear temporal interpolation between the responses $\tilde{u}_n(R,\psi_i,z,t)$ is build. This interpolation is based on the main assumptions previously described in this paper, and more particularly one on those stating on the axisymmetric condition of the ring gear and the invariability of the modal basis whatever the position of the planet axis. On the time interval $t_i \leq t \leq t_{i+1}$, the following linear time interpolation scheme can be written:

$$u_n(R,\varphi_n,z,t) = \frac{\tilde{u}_n(R,\varphi_n - \Omega_c t_i,z,t)(t_{i+1} - t) + \tilde{u}_n(R,\varphi_n - \Omega_c t_{i+1},z,t)(t - t_i)}{(t_{i+1} - t_i)} \tag{15}$$

From a practical point a view, the iterative spectral method gives access to the answers in discrete nodes of the ring gear $\tilde{u}_i(R,\psi = \psi_i,z,t)$, $i = 1$ à P (54 points considered in our application). Thus, the answer $u_n(R,\varphi_n,z,t))$ is evaluated at the node of the model identified by $\varphi_k = 2k\pi/P$ $(k = 0,1,...,P-1)$. By properly choose time interval and ring gear discretization, and by considering that all the nodes on a peripheral circle of the ring gear have an identical response to within one phase, the dynamics response of the node identified by the angle $\varphi_k = 0$ at time t is equal to:

$$\begin{aligned} u_n(R,0,z,t) = \Omega_{kc} \sum_{i=0}^{P-1} \left[\tilde{u}_i(R,\frac{2\pi(P-i)}{P},z,t)(t_{i+1} - t) + \tilde{u}_i(R,\frac{2\pi(P-1-i)}{P},z,t)(t - t_i) \right] \\ \times \mathrm{H}(t - t_{i+1})\mathrm{H}(t_i - t) \end{aligned} \tag{16}$$

with H the Heaviside function.

3 Numerical results

The studied planetary gear set has the sun as its input and the carrier as the output, so that the ring gear remains fixed. Its main characteristic are given in Table 1.

Table 1: Main characteristics of the studied planetary gear set

	Sun	Planets	Ring
Number of planets N	3		
Number of teeth Z	27	40	108
Module m_o	1.5		
Pressure angle α (°)	20		
Helix angle β (°)	0		
Transmission ratio 1	5		

Based on the gear module, the maximum permissible input torque is 156 Nm, i.e. a breaking torque of $780\ Nm$. The nominal input operating speed of the planetary gear is $1500\ rpm$, with a maximum operating speed of $3500\ rpm$. A test bench is instrumented to allow the vibratory and acoustical characterization of planetary gear sets, such as instantaneous rotational speed of input and output gearbox shafts, the radial acceleration of planetary gear housing and the radiated noise. This allows direct comparison with numerical results at each computational step [17]. In this paper, the focus will be on the radial acceleration of planetary gear housing to validated the capacity of the proposed method to access housing modulated vibratory response.
In this application, the applied motor torque is equal of $100\ Nm$ and the excitation spectra (STE and mesh stiffnesses fluctuations) include the first six harmonics of the mesh frequency. The modal equivalent modal damping rate is chosen to be uniform across all modes and is equal to 5%. Finally, the ring gear is supposed to be perfectly cylindrical (and so perfectly axisymmetric). Indeed, the small variation of ring gear thickness observed on the real system induced negligible deviation in modal basis and dynamic response.
Two test cases will be discussed. First, the dynamic response at low speed ($250\ rpm$) is computed, when the harmonics of the mesh frequency are lower than the eigenfrequencies of the system. Then, the dynamic response at high speed ($3100\ rpm$) is computed, when the harmonics of the mesh frequency may coincide with frequencies for which the ring gear exhibits significant operational dynamic deformation. Hight speed measurement result are finally discussed to evaluate the relevance of the proposal numerical model. For both results, special attention is given to modulation shape of the radial acceleration of housing (ring gear) over a complete carrier rotational period T_c.

3.1 Dynamic response of the ring gear at low speed

The dynamic response of the ring gear is evaluated for a sun rotation speed of $250\,rpm$. The mesh frequency is then equal to $f_m = 90\ Hz$. At low rotational speeds, the first harmonics of the mesh frequency are lower than the natural frequencies of the system, thus the ring gear responds on its static deformation, i.e. the static contribution of the modes. This static deformation is calculated by considering unitary forces directed along the lines of action, as shown on Figure 4(a). This induced a deformation composed of six lobes, that can be express as a function A_s describing the amplitude of the static deformation in polar coordinate, as shown in Figure 4(b).Figure 4(c, d) show temporal response of the radial acceleration of the ring gear dynamic response for a complete carrier rotation T_c, for purely harmonic excitation at the mesh frequency H_{108}, and its associated spectrum, plotted as a function of the output frequency order (carrier frequency) around the range of order from 100 to 116. If the model was perfectly axisymmetric, one would observed a periodic temporal response with a period equal to $T_c/3$, corresponding to the periodic passage of the three planets. In our application test case, ones can observed a slightly different behaviour because the system isn't perfectly axisymmetric. The spectrum has a moderate amplitude at the mesh frequency f_m. The dominant lines are the sidebands at $f_m \pm N$, where N is the number of planets. Ones also observe that the envelope of the temporal response has six lobes, reflecting the amplitude modulation phenomena. Detailed analysis of the time response envelope for this operating regime allows a link to be established between

its amplitude and the static deformation of the ring gear. This result shows a different behaviour from those usually found in the literature with simplified formulation, when the modulated signal is only considered as a growth/decay of the vibratory amplitude as one planet approaches or moves away, which would lead for our application case to a three-lobe signal [9].

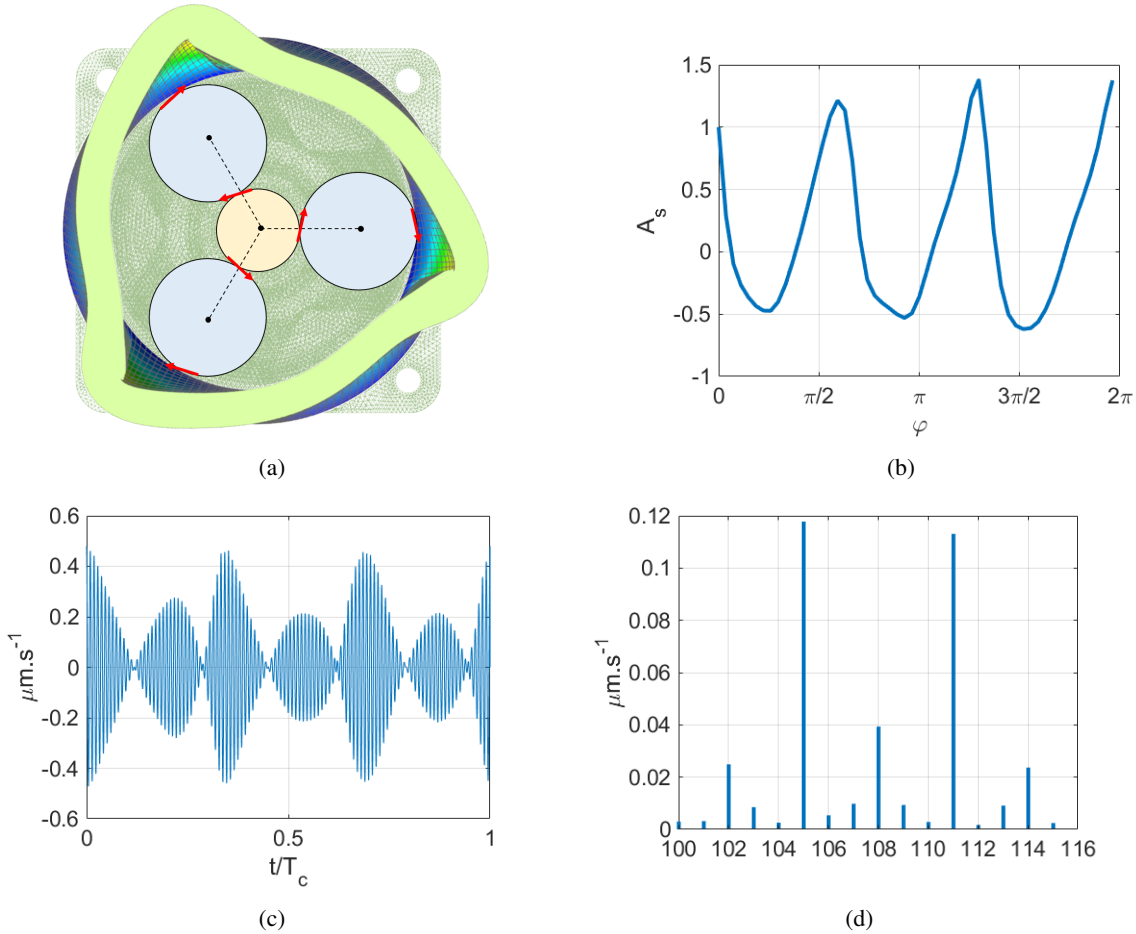

Figure 4: (a) Static deformation of the ring gear induced by unitary force oriented along the line of action. (b) Adimensionnal amplitude of the static deformation in polar coordinate. (c) Temporal response of the radial acceleration of the ring gear dynamic response for a complete carrier rotation. (d) Amplitude spectra in function of the mesh frequency order.

3.2 Dynamic response of the ring gear at high speed

For high operating regimes, the higher order harmonics of the mesh frequency are high enough to coincide with the eigenmodes of the system. The dynamic response of the ring gear is considered for a sun rotation speed equal to $3100\ rpm$. The mesh frequency is then equal to $1116\ Hz$.

Figure 5(a) shows the time evolution of the modulated dynamic response of the ring gear and figure 5(d) the amplitude spectrum, plotted as a function of the carrier frequency order. An amplification of the fifth and sixth harmonics of the mesh frequency is observed, corresponding to an excitation of the modes around 5580 and $6695\ Hz$. We propose to analyse the dynamic response extracted around these two harmonics. Figures 5(b, c) show the corresponding temporal evolutions. Figures 5(e, f) show the amplitude spectra associated, plotted as a function of the output frequency order (carrier frequency) around the order range from 532 to 548 on one hand, and from 640 to 656 on the other hand. As with the low-speed dynamic response, the amplitude of the harmonics of the mesh frequency H_{540} and H_{648} are lower than that of the sidebands at $H_{108}i \pm NH_1$ and $H_{108}i \pm kH_1$, with N the number of planets and k an integer. The shape of the envelope of the temporal dynamic responses is complex and

depends on the frequency of observation, and so on the modes exited. Futhermore, the number of lobes seems to be driven by the difference between the two most significant sidebands. For example, we observe six lobes for the dynamic response around the fifth harmonic (driven by the sidebands $H_{537}$and H_{543}), while we observe four lobes for the dynamic response around the sixth harmonic (driven by the sidebands H_{645} andH_{649}). Moreover, one should observed that the periodic temporal response with a period equal to $T_c/3$ observed at low speed is no longer representative of the modulated signal. Here again, numerical results show a behaviour far to be representative to a three lobe temporal evolution of the ring gear radial acceleration.

In order to validate the relevance of the numerical results from the new method proposed in this paper, experimental results for hight rotational speed are analysed. Here, the complexity lies in the quality of the tunning of the numerical model compared to measurement. Indeed, a frequency shift of the modes, a poorly estimated modal damping or geometrical simplifications of the numerical model make it difficult to choose the rotational speed which would give us exactly the same operational deformation shape both in simulation and in measurement. In the present paper, numerical rotational speed and measurement one are choose to give a qualitative comparison of the phenomena that drive the modulated vibratory response of a planetary gearbox without trying an quantitative comparison.

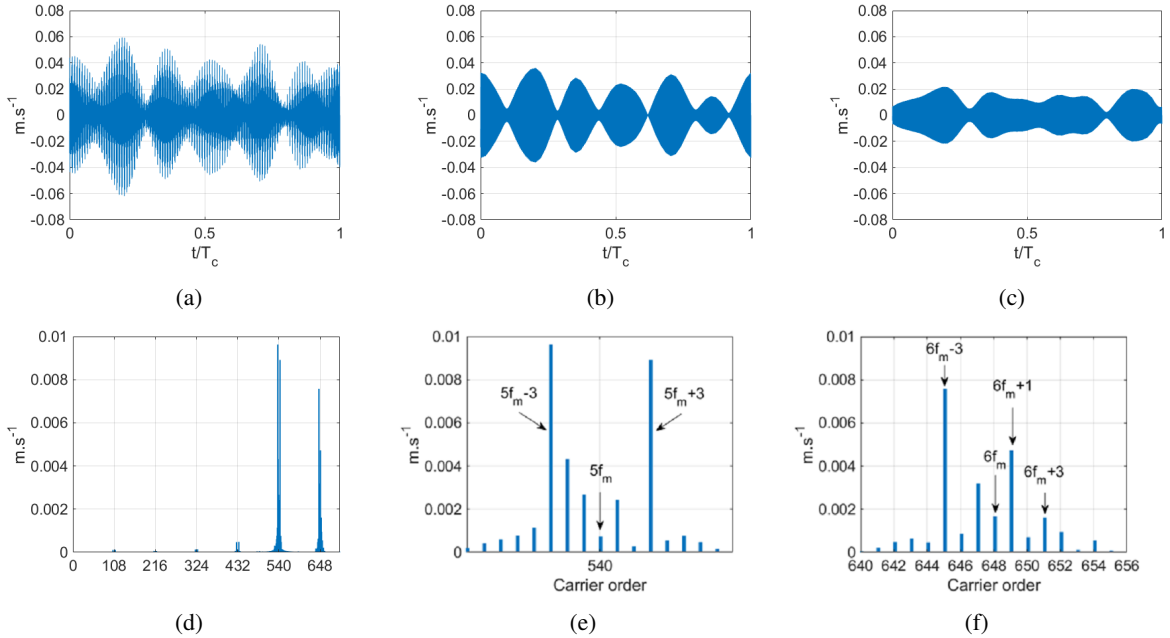

Figure 5: (a) Temporal evolution of the overall ring gear dynamic response. (b) Temporal evolution of the ring gear dynamic response on the order range [532 548]. (c) Temporal evolution of the ring gear dynamic response on the order range [640 656]. (d) Amplitude spectra of the overall ring gear dynamic response. (e) Amplitude spectra of the ring gear dynamic response on the order range [532 548]. (f) Amplitude spectra of the ring gear dynamic response on the order range [640 656].

The quasi-axisymmetric boundary conditions of the ring gear are experimentally well verified. Thus, the experimental results presented below are the algebraic mean value of the levels measured by the different accelerometers. The global level measured experimentally includes phenomena not considered in the numerical model (friction, assembly errors, etc.). For the comparison between computation and measurement, the dynamic responses are extracted around the first four harmonic of the mesh frequency, included sidebands induced by carrier rotation.
As an example, the experimental dynamic response measured at 800 and at $2200\,rpm$ is presented in Figure 6(a, b) retaining only the frequency contributions on the order band $H_{108}i \pm NH_1$, (i=1, 2, ...6), N being the number of planets. We observe a signal with a complex modulation, with a high number of sidebands at the mesh frequency. Qualitatively, one observes 6 lobes at 800 and $2200\,rpm$. The zero crossing of the dynamic response is only visible when the dynamic response is plotted by only retaining an order band around a particular harmonic (see 6(c, d)). It is also observed in this figure that the dynamic response at 800 rpm, retaining only the frequency contributions on

the order band $H_{216} \pm 3H_1$, shows a number of lobes equal to 5, whereas at 2 200, by retaining only the frequency contributions on the order band $H_{432} \pm 3H_1$, we observe 6 lobes. The experimental observations are qualitatively consistent with what is observed numerically (see the digital application).

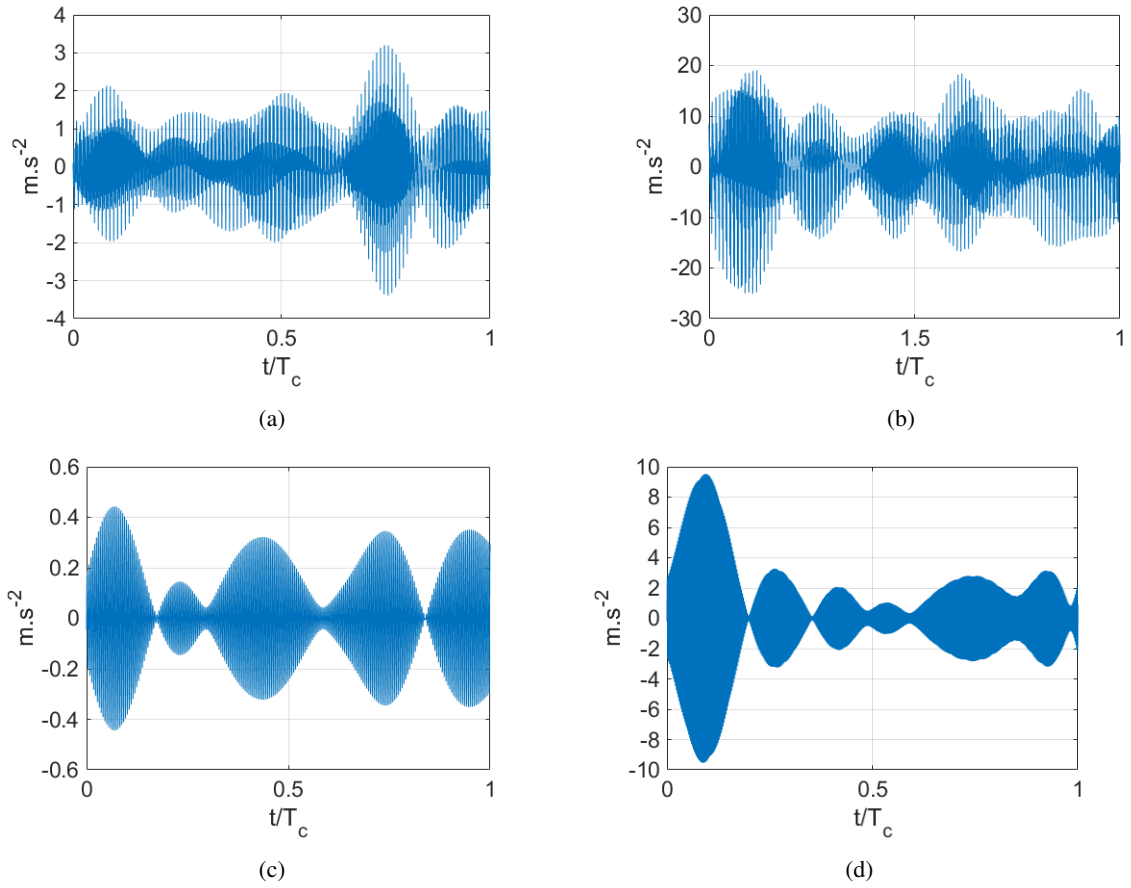

Figure 6: (a) Ring gear dynamic response measured at 800 rpm. (b) Ring gear dynamic response measured at 2200 rpm. (c) Ring gear dynamic response measured at 800 rpm, order 2 of the mesh frequency. (d) Ring gear dynamic response measured at 2200 rpm, order 4 of the mesh frequency

The observation of number of lobes performed here illustrated than conventional simplified analytical formulation to modulate the dynamic response of the ring gear failed to be representative of the complexity of this phenomena. By integrating modal behaviour in the modulation numerical model, based on non-modulated initial signal, one can reach a richer dynamic response, where an acoustic transcription of which would be closer to the real sound of the planetary gearbox.

4 Conclusion

The modulated dynamic response of the ring gear of the planetary gear is evaluated using an original approach which considers its operational deformation for each operating regime. Analysis of numerical and experimental results is based one observation of the number of lobes over a complete carrier rotational period. If this analysis don't statued on the quantitative capability of the propose model, it shows how taking into account the modal behaviour of the system during converting a non-modulated signal to a modulated one can reach a more complex dynamic response, correlated to experimental observation.
The numerical results show that for low sun rotation speeds, the envelope of the dynamic response of the ring gear is driven by the static deformation of the planetary gear. At higher rotational speeds, when the harmonics of the mesh frequency are high enough to coincide with the eigenmodes of the system, the envelope of the modulated dynamic response is driven by the operational deformation of the ring gear. Measurement investigations confirm that the modulated dynamic response of the ring gear can presented more lobes than the number of planet.

The used of the spectral iterative method offer low computational time and give the opportunity to extract the dynamic response at several points to construct a refine modulated response. It also offer the opportunity to performed parametrical simulation, key of a better understanding of ring gear modulation dynamic responses effects and improving numerical model.

Acknowledgment

References

[1] D. B. Welbourn, "FUNDAMENTAL KNOWLEDGE OF GEAR NOISE: A SURVEY," 1979.

[2] S. L. Harris, "Dynamic Loads on the Teeth of Spur Gears," *Proceedings of the Institution of Mechanical Engineers*, vol. 172, pp. 87–112, June 1958.

[3] E. Rigaud and J. Sabot, "Effect of Elasticity of Shafts, Bearings, Casing and Couplings on the Critical Rotational Speeds of a Gearbox," Jan. 2007. arXiv:physics/0701038.

[4] A. Carbonelli, E. Rigaud, and J. Perret-Liaudet, "Vibro-Acoustic Analysis of Geared Systems—Predicting and Controlling the Whining Noise," in *Automotive NVH Technology* (A. Fuchs, E. Nijman, and H.-H. Priebsch, eds.), pp. 63–79, Cham: Springer International Publishing, 2016. Series Title: SpringerBriefs in Applied Sciences and Technology.

[5] P. D. McFadden and J. D. Smith, "An Explanation for the Asymmetry of the Modulation Sidebands about the Tooth Meshing Frequency in Epicyclic Gear Vibration," *Proceedings of the Institution of Mechanical Engineers, Part C: Journal of Mechanical Engineering Science*, vol. 199, pp. 65–70, Jan. 1985.

[6] J. McNames, "Fourier Series Analysis of Epicyclic Gearbox Vibration," *Journal of Vibration and Acoustics*, vol. 124, pp. 150–153, Jan. 2002.

[7] J. Perret-Liaudet, "AN ORIGINAL METHOD FOR COMPUTING THE RESPONSE OF A PARAMETRICALLY EXCITED FORCED SYSTEM," *Journal of Sound and Vibration*, vol. 196, pp. 165–177, Sept. 1996.

[8] J. Neufond, E. Denimal, E. Rigaud, J. Perret-Liaudet, and A. Carbonelli, "Whining noise computation of a planetary gear set induced by the multi-mesh excitations," *Proceedings of the Institution of Mechanical Engineers, Part C: Journal of Mechanical Engineering Science*, vol. 233, pp. 7236–7245, Nov. 2019.

[9] M. Inalpolat and A. Kahraman, "A theoretical and experimental investigation of modulation sidebands of planetary gear sets," *Journal of Sound and Vibration*, vol. 323, pp. 677–696, June 2009.

[10] D. F. Plöger, C. Fischer, and S. Rinderknecht, "Linking the modulation of gear mesh vibration in planetary gearboxes to manufacturing deviations," *Mechanical Systems and Signal Processing*, vol. 155, p. 107554, June 2021.

[11] M. S. Tavakoli and D. R. Houser, "Optimum Profile Modifications for the Minimization of Static Transmission Errors of Spur Gears," *Journal of Mechanisms, Transmissions, and Automation in Design*, vol. 108, pp. 86–94, Mar. 1986.

[12] E. Rigaud and D. Barday, "Modelling and Analysis of Static Transmission Error. Effect of Wheel Body Deformation and Interactions between Adjacent Loaded Teeth," 1999.

[13] S.-J. Tsai, G.-L. Huang, and S.-Y. Ye, "Gear meshing analysis of planetary gear sets with a floating sun gear," *Mechanism and Machine Theory*, vol. 84, pp. 145–163, Feb. 2015.

[14] R. G. Parker and J. Lin, "Mesh Phasing Relationships in Planetary and Epicyclic Gears," *ASME*, vol. 2003, pp. 525–534, 2003.

[15] C. G. Cooley and R. G. Parker, "Vibration Properties of High-Speed Planetary Gears With Gyroscopic Effects," *Journal of Vibration and Acoustics*, vol. 134, p. 061014, Oct. 2012.

[16] J. Neufond, Y. Xu, J. Perret-Liaudet, and E. Rigaud, "The iterative spectral method for computing the planetary gear dynamic response," in *International Conference on Gears 2017* (VDI Wissensforum GmbH, ed.), pp. 209–218, VDI Verlag, 2017.

[17] J. Neufond, E. Rigaud, J. Perret-Liaudet, and A. Carbonelli, "Influence of tooth profile modifications on the dynamic behavior of a planetary gear set – Experimental investigation and numerical validation for different amplitudes of tooth profile modifications," in *International Conference on Gears 2019* (VDI Wissensforum GmbH, ed.), pp. 765–776, VDI Verlag, 2019.